Noiseless Optical Amplifier Operating on Hundreds of Spatial Modes

N. V. Corzo, A. M. Marino, K. M. Jones, and P. D. Lett

Phys. Rev. Lett. **109**, 043602 — Published 26 July 2012

DOI: 10.1103/PhysRevLett.109.043602

Noiseless optical amplifier operating on hundreds of spatial modes

N. V. Corzo[1,2], A. M. Marino[1], K. M. Jones[3], and P. D. Lett[1*]
[1] *Quantum Measurement Division, National Institute of Standards and Technology, and Joint Quantum Institute, NIST and University of Maryland, 100 Bureau Dr., Gaithersburg, MD 20899-8424*
[2] *Departamento de Física, Centro de Investigación y Estudios Avanzados del Instituto Politécnico Nacional, México D.F., 07360, México*
[3] *Department of Physics, Williams College, Williamstown, Massachusetts 01267 USA*
(Dated: June 1, 2012)

We implement a noiseless optical amplifier using a phase-sensitive four-wave mixing process in rubidium vapor. We observe performance near the quantum limit for this type of amplifier over a range of experimental parameters, and show that the noise figure is always better than would be obtained with a phase-insensitive amplifier with the same gain. Additionally, we observe that the amplifier supports hundreds of spatial modes, making it possible to amplify complex two-dimensional spatial patterns with less than a 10 % degradation of the input signal-to-noise ratio for gains up to 4.6. To confirm the multi-mode character of the amplifier we study the noise figure as a function of spatially-varying losses. Additionally we investigate the spatial resolution of the amplifier and show that it supports a range of spatial frequencies from 1.3 to over 35 line pairs per millimeter.

Optical amplifiers offer the potential to significantly improve the performance of systems in a range of fields including optical communications, quantum information processing, continuous-variable quantum computing, enhancement of optical resolution and image amplification [1–5]. It is important, for practical applications, that they add as little noise as possible to the signal they amplify. The most common type of optical amplifier is the phase-insensitive amplifier (PIA), which is a linear amplifier whose gain and noise are independent of the phase of the input signal. The output of such an amplifier necessarily has a lower signal-to-noise ratio (SNR) than the input and the level of degradation depends on the gain. In contrast, a phase-sensitive amplifier (PSA) is a linear amplifier whose gain and noise do depend on the phase of the input signal. For the correct choice of the input phase the PSA does not degrade the SNR, independent of the gain. In this sense, the PSA behaves as a noiseless amplifier. The quantum noise properties of both of these optical amplifiers are well understood theoretically [6–8], but there have been few experimental implementations. PSAs that have been successfully realized have employed $\chi^{(2)}$ non-linear crystals [9–13] and single mode $\chi^{(3)}$ non-linear fibers [14–18].

The ability to implement a PSA that can simultaneously amplify multiple spatial modes allows noiseless image amplification, which is an important goal in imaging research [19–21]. Although $\chi^{(2)}$-based optical parametric amplifiers (OPAs) have been used to implement a multi-spatial-mode PSA, they require the high peak power of a pulsed laser because of low gain [4, 11, 12]. Attempts have also been made to implement an optical parametric oscillator (OPO) that can support many spatial modes using a degenerate optical cavity [13]. In each case, the main constraint has been the limited number of modes supported by the amplifier.

In this letter we report on a PSA that can support at least hundreds of spatial modes, making it possible to noiselessly amplify complicated two-dimensional images for the first time, to our knowledge. This is made possible by the large $\chi^{(3)}$ response that can be obtained using an atomic vapor and near-resonant light. We use a four-wave mixing (4WM) process in Rb vapor to achieve phase-sensitive amplification in a double-Λ configuration. The multi-spatial mode nature arises from the relaxed phase-matching conditions of the 4WM due to a short cell, making it possible to amplify a large range of probe wave vectors. In addition a large $\chi^{(3)}$ results in a large single-pass gain that makes it possible to implement the PSA without a cavity. These properties were also the basis for the multi-spatial mode properties of the 4WM-based PIA of Ref. [22].

In the 4WM process two strong pump fields and a weak probe field are mixed in the atomic medium, as shown in Fig. 1. This leads to the conversion of one photon from each pump into two photons of the probe, or vice versa, depending on the relative phases between each of the pumps and the probe. As the relative phases are changed, the gain G can take values of $G > 1$ (amplification) or $G < 1$ (deamplification). Only for two conditions on the relative phases does the PSA preserve the input SNR. Defining the phases for the two pumps and the probe as θ_1, θ_2, and θ_p the conditions are: $2\theta_p - \theta_1 - \theta_2 = [0, \pi]$, and these coincide with the maximum deamplification and maximum amplification of the input [9], respectively. The double-Λ scheme used for the 4WM allows us to overcome sources of excess noise, such as spontaneous emission. This made it possible for us to demonstrate that this system can generate a vacuum single-beam quadrature squeezed state containing at least a few spatial modes [23]. While our previous work only offered a proof of the multi-spatial mode nature of the 4WM process, in this paper we show that when operating as an amplifier the device can support a

significantly larger number of spatial modes than previous reported systems [4, 12, 13] while still operating as a noiseless amplifier.

The configuration and experimental setup is similar to the one described in [23] and is shown in Fig. 1. We use a single Ti:Sapphire ring laser to generate a probe beam at frequency ν_p, detuned to the blue of the ^{85}Rb $5S_{1/2}, F = 3 \rightarrow 5P_{1/2}$ transition with a one-photon detuning $\Delta = 0.9$ GHz, as shown in the inset to Fig. 1. From the same laser, we derive the two different pump frequencies (ν_1 and ν_2) by frequency-shifting the light (ν_1 to the red and ν_2 to the blue of ν_p) with two double-passed 1.52 GHz acousto-optic modulators (AOMs), giving a two-photon detuning δ of -4 MHz (as defined in Fig. 1). The beams out of the AOMs are used to seed two tapered amplifiers whose outputs are spatially-filtered and contain up to 225 mW each. These beams have the same linear polarization which is orthogonal to the polarization of the probe. The two pumps and the probe are combined on a polarizing beam splitter (PBS) with an angle of 0.4 degrees between the pump beams (the probe beam bisects the angle of the pumps as shown in Fig. 1). The three beams intersect in a 12.5 mm vapor cell filled with isotopically pure ^{85}Rb. The cell, with no magnetic shielding, is heated to $\approx 86°$C. The pumps and probe are collimated with waists of 600 μm and 250 μm ($1/e^2$ radius), respectively, at the center of the cell. After the PSA, the output probe is separated from the pump beams with another PBS.

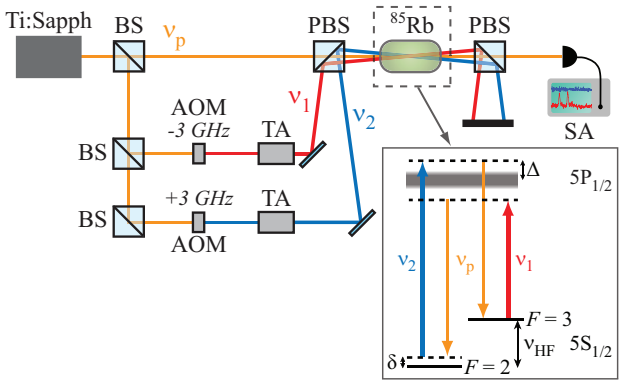

FIG. 1. (Color online) Experimental setup for the 4WM-based PSA in hot ^{85}Rb vapor. AOM: acousto-optic modulator, TA: semiconductor tapered amplifier, SA: radio-frequency spectrum analyzer, PBS: polarizing beam splitter, BS: beam splitter. Inset: Energy level diagram for the double-Λ system. The width of the excited state represents the Doppler broadened line, Δ is the one-photon detuning, δ is the two-photon detuning, and ν_{HF} is the hyperfine splitting.

We characterize the performance of the PSA in terms of the noise figure (NF), which is defined as the ratio between the SNR of the input ($\mathrm{SNR_{IN}}$) and the output ($\mathrm{SNR_{OUT}}$) signals:

$$\mathrm{NF} = \frac{\mathrm{SNR_{IN}}}{\mathrm{SNR_{OUT}}}. \tag{1}$$

An ideal PIA has a $\mathrm{NF_{PIA}} = 2 - 1/G_{\mathrm{PIA}}$, where G_{PIA} is the intensity gain. On the other hand, for the correct phase an ideal PSA has a NF $= 1$ independent of the gain. For a total detection efficiency $\eta < 1$ the measured NF can suffer from overestimation and result in a value below the ideal NF. For the PSA this can lead to a NF less than one. This is because the SNR of a shot-noise-limited input is degraded more with losses than the SNR of the amplified output. Furthermore, this behavior depends on the type of optical amplifier, PSA or PIA, and on the amplifier gain, as follows:

$$\mathrm{NF_{PIA}} = \eta \left[2 - \frac{2}{G_{\mathrm{PIA}}} + \frac{1}{\eta G_{\mathrm{PIA}}} \right] \tag{2}$$

$$\mathrm{NF_{PSA}} = \eta \left[1 - \frac{1}{G_{\mathrm{PSA}}} + \frac{1}{\eta G_{\mathrm{PSA}}} \right], \tag{3}$$

where G_{PSA} and G_{PIA} are the phase-sensitive and the phase-insensitive gains for a single mode, respectively.

Following the method described in [24, 25], the input signal to our PSA comes from amplitude modulating a 20 μW probe with an AOM at a frequency of 1 MHz with a SNR of 20 dB. The SNR is measured with a radio frequency spectrum analyzer centered at 1 MHz with a resolution bandwidth of 3 kHz and a video bandwidth of 100 Hz. The $\mathrm{SNR_{IN}}$ is measured by bypassing the vapor cell using flip mirrors. The relative phases are locked using the system described in [23]. From the measured amplitudes of the input and output modulation peaks we calculate the gain of the system at 1 MHz.

When measuring the input and output SNR using an intensity detector, it is essential to check that the input signal contains purely amplitude modulation. If the input contains any phase modulation the input SNR can be underestimated and the maximum output intensity modulation may be obtained when $2\theta_p - \theta_1 - \theta_2 \neq \pi$. This is a result of a mixing of the quadratures that occurs during the amplification process when the phase difference is not π. As a result, it is possible to obtain a larger output signal than the one that would be obtained for an input with only amplitude modulation, which can lead to an apparent NF smaller than that of an ideal PSA.

Using the 4WM-based amplifier we have measured a NF of 0.98 ± 0.01 with a gain of 3.9 ± 0.1 at $\Delta = 0.9$ GHz and $\delta = -4$ MHz. (The indicated uncertainties represent one standard deviation, combined statistical and systematic uncertainties.) For our experiment, the total detection efficiency of the system is 91 % which comes from the optical path transmission (96 %) and the photodiode efficiency (95 %). Using a gain of 3.9 in Eqs. (2) and (3) the NFs for an ideal PIA and PSA are 1.6 and 0.93, respectively. Thus, the PSA operates close to the quantum limit, and much better than an ideal PIA.

The gain of the amplifier can be changed without a significant degradation of its properties. We first vary the one-photon detuning Δ. Figure 2(a) shows the measured gain of our PSA for different values of Δ. Figure 2(b) shows the measured NF (red circles) and the expected NF for an ideal PIA (blue line) and an ideal PSA (green line) given the measured gain of the amplifier and the detection efficiency given above. The measured NF of the 4WM-based PSA is better than the expected one for a PIA, with the same gain, and close to the ideal PSA over a large range of Δ, from 0.9 GHz to 2.2 GHz. The biggest difference between the measured NF and NF_{PIA} occurs at $\Delta = 0.9$ GHz, which also corresponds to the highest gain (around 4) with good NF.

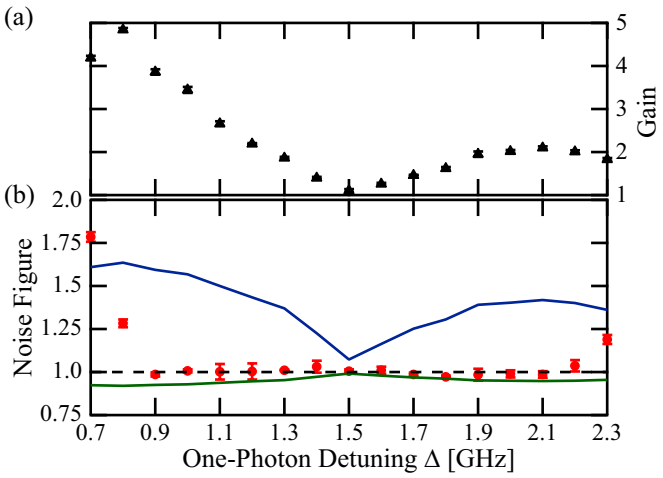

FIG. 2. (Color online) Measured (a) gain and (b) NF (red circles) for the PSA at 1 MHz as a function of one-photon detuning Δ. The green and blue lines show the theoretical NF for an ideal PSA and PIA, respectively, calculated using the measured gain at each value of Δ and the experimental detection efficiency.

We observe that the NF of the PSA deteriorates near the atomic resonances, for detunings lower than 0.9 GHz or higher than 2.2 GHz. This is due to absorbtion and extra 4WM processes that become stronger near resonance and add uncorrelated noise to the PSA's output. These are the same processes that limited the squeezing levels in [23]. In particular, the phase-insensitive 4WM process described in [25, 26] has been observed in our experiment for $\Delta < 0.9$ GHz and $\Delta > 2.3$ GHz and represents one of the main sources of excess noise. In this process the probe beam interacts with only one of the pumps and an extra beam is generated on the other side of the pump.

The gain of the PSA can be changed by increasing the temperature of the cell. This also causes the extra 4WM processes to become stronger and leads to a degradation of the NF. We have observed that the PSA preserves its noiseless operation for a range of temperatures between 78°C to 86°C. In this region the gain of the PSA increases as we increase the temperature and the NF remains close to the quantum limit. Beyond those temperatures, the NF starts to deteriorate. At even higher temperatures (≈ 94°C) the gain starts to decrease as well.

One of the most important properties of our PSA is its multi-spatial-mode character. In order to investigate this property, we seed the PSA with different spatial patterns. The patterns are created with an opaque amplitude mask in the path of the probe beam and imaged into the amplifier. The highest spatial frequencies of the input probe, which are not supported by the amplifier, are removed with a spatial filter placed before the PSA. After amplification the output is imaged at the detector. There, the photodiode integrates over the spatial profile of the image and the NF is measured as described above, by amplitude modulating the input beam at 1 MHz and measuring the SNR at this frequency. The inset of Fig. 3 shows a particular example of an "N"-shaped pattern before and after the amplifier. For this particular case we have observed a NF as low as 0.98 ± 0.01 with a gain of 4.6 ± 0.1 at $\Delta = 0.9$ GHz and $\delta = -4$ MHz (For the rest of the paper these values of Δ and δ are unchanged). The total detection efficiency in this case is 88 %, due to the additional imaging system and a spatial filter after the amplifier which is meant to reduce the scattered pump light. With this detection efficiency and the measured gain, the theoretical NF for the ideal PSA and PIA are 0.90 and 1.59, respectively. The fact that the PSA preserves the NF for different spatial patterns is an indication of its multi-spatial-mode character.

A way to discriminate between single- and multi-mode operation is to examine the dependence of the NF on spatially-varying losses. For a single-spatial-mode PSA, the NF measured after any loss, independent of its origin, should scale linearly, as in Eq. (3). Any deviation from this behavior is an indication of multi-spatial-mode behavior. To study this we spatially cut the "N"-shaped image after the amplifier in different ways and measure the NF as a function of transmission. This spatial cutting is done at an image plane after the cell.

We first attenuate the amplified output using a neutral density (ND) filter over the whole image. This should lead to a linear behavior of the NF similar to Eq. (3) since all the modes are equally attenuated. Figure 3 shows the measured NF (blue squares) as function of the normalized measured intensity for this case. In addition, the figure shows a linear fit (blue line) to the measured NF. For the fit we fix the value of the slope to that from Eq. (3) using the measured gain of $G_{PSA} = 4.6$, but we allow for the value of the NF at $\eta = 1$ to be different than one to take into account any imperfections in the PSA. As expected, the measured NF follows a linear behavior. We also measure the NF when we clip the PSA output with a slit from both sides (red circles). In this case the NF begins by following the ideal single-mode PSA as the transmission decreases up to ≈ 70 %. After that point

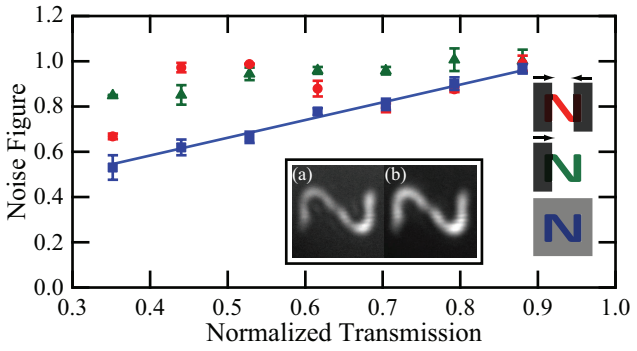

FIG. 3. (Color online) NF measurements at 1 MHz as a function of spatially-varying losses when cutting with a slit (red circles), cutting with a razor blade (green triangles), or attenuating with an ND filter (blue squares). The blue line shows a linear fit to the measured NF when attenuating with an ND filter. The slope of the fit is given by Eq. (3) for a single-mode PSA. The normalized transmission incorporates the detection efficiency of 88 %. The inset shows (a) the input image and (b) the amplified output image for the letter "N".

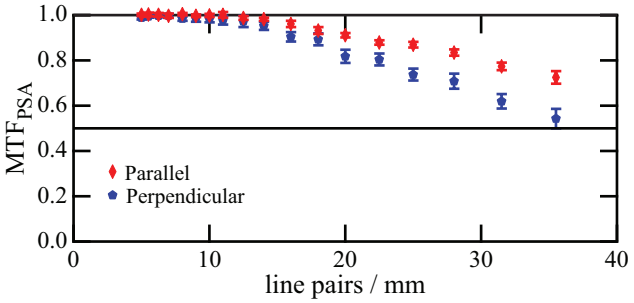

FIG. 4. (Color online) Modulation transfer function of the PSA ($\mathrm{MTF_{PSA}}$) measured along two spatial directions: parallel to the plane defined by the pumps (red diamonds) and perpendicular to this plane (blue pentagons). The spatial frequencies are measured inside the 4WM cell.

the behavior deviates completely from the one expected for a single-mode system. Finally, we measure the NF when we clip with a razor blade from only one side (green triangles). In this case the NF decreases as the normalized transmission decreases, but not at the same rate as with the ND filter. Although a greater knowledge of the mode structure of the PSA is needed to fully understand the results shown in Fig. 3, the difference in behavior between the three different methods of spatially masking the output beam is a signature of the multi-mode nature of the PSA.

In order to perform a detailed study of the spatial resolution of our PSA we measure the modulation transfer function (MTF) of the system. We seed the amplifier with different spatial frequencies taken from a resolution target. The target is imaged inside the cell with a magnification of 1/5. A second optical system then images the cell onto a CCD camera. We normalize the MTF of the system including the PSA to that of the system without the PSA to remove the contribution from the optical system and obtain the $\mathrm{MTF_{PSA}}$ of the amplifier alone. In Fig. 4 we plot the $\mathrm{MTF_{PSA}}$ for the directions parallel and perpendicular to the plane defined by the pump beams. The spatial frequencies are those inside the 4WM cell. For low spatial frequencies, from 5 lp/mm (line pairs per millimeter) to 15 lp/mm, the PSA maintains a $\mathrm{MTF_{PSA}}$ close to one. The $\mathrm{MTF_{PSA}}$ decreases to 0.5 only for frequencies higher than 35 lp/mm. This compares well with previous results reporting amplification of spatial frequencies up to 10 lp/mm in a nonlinear crystal [12].

To get an estimate of the number of modes supported by the amplifier, we measure the area of the gain region inside the PSA. We do this by seeding the amplifier with a probe whose waist is much larger than the pump beams inside the cell. This results in amplification over a small region of the input probe, which we measure by comparing the probe beam with and without gain from the PSA. We define the field gain area as the region over which $(\sqrt{G_{\mathrm{PSA}}} - 1)$ is above half of its maximum value and measure this area to be approximately $\pi(0.37\ \mathrm{mm})^2 = 0.43\ \mathrm{mm}^2$. Using this gain area and the spatial resolution of the PSA of at least 35 lp/mm, following Ref. [27] we calculate a spatial bandwidth product ($\pi[0.37\ \mathrm{mm} \times 2 \times 35\ \mathrm{lp/mm}]^2$) of over 2000. Using other methods [21] leads to even larger estimates of the number of independent spatial modes for the PSA. These numbers are significantly larger than what has been achieved with quantum limited PSAs using nonlinear crystals [4, 12, 13] and make it possible to noiselessly amplify complicated two-dimensional images without a significant degradation of their resolution.

We have presented a study of "noiseless" amplification using a phase-sensitive 4WM process in Rb vapor. Performance near the quantum limit for a range of parameters is observed. We show that the PSA supports different spatial modes without a significant degradation of the SNR, with a NF of 0.98 ± 0.01 with a gain of 4.6 ± 0.1 and a detection efficiency of 88 % for an "N"-shaped beam. We have verified the multi-spatial-mode behavior of the amplifier by studying the NF as a function of spatially-varying losses. Finally, we have studied the spatial resolution by measuring the MTF of the amplifier and found that it can support spatial frequencies higher than 35 lp/mm. This result, combined with a measurement of the area of the gain region, allowed us to show that the PSA can support a significantly larger number of spatial modes in both transverse directions than previous PSAs constructed using parametric crystals [4, 12, 13]. A natural extension of this work will be to study the effect of the PSA directly on the spatial

fluctuations of a single shot image.

This work was supported by the DARPA, AFOSR and NSF (PFC @ JQI). N.V.C. acknowledges CONACYT.

* paul.lett@nist.gov

[1] S. L. Braunstein and P. van Loock, Rev. Mod. Phys. **77**, 513 (2005).
[2] S. Fossier, E. Diamanti, T. Debuisschert, R. Tualle-Brouri, and P. Grangier, J. Phys. B **42**, 114014 (2009).
[3] M. I. Kolobov, *Quantum imaging* (Springer, 2007).
[4] O. K. Lim *et al.* Proc. of SPIE **8163**, 816306 (2011).
[5] C. A. Santivanez *et al.* Proc. of SPIE **8163**, 81630Z (2011).
[6] W. H. Louisell, A. Yariv, and A. E. Siegman, Phys. Rev. **124**, 1646 (1961).
[7] H. A. Haus and J. A. Mullen, Phys. Rev. **128**, 2407 (1962).
[8] C. M. Caves, Phys. Rev. D **26**, 1817 (1982).
[9] J. A. Levenson, I. Abram, T. Rivera, and P. Grangier, J. Opt. Soc. Am. B **10**, 2233 (1993).
[10] Z. Y. Ou, S. F. Pereira, and H. J. Kimble, Phys. Rev. Lett. **70**, 3239 (1993).
[11] A. Mosset, F. Devaux, and E. Lantz, Phys. Rev. Lett. **94**, 223603 (2005).
[12] S. K. Choi, M. Vasilyev, and P. Kumar, Phys. Rev. Lett. **83**, 1938 (1999).
[13] L. Lopez, N. Treps, B. Chalopin, C. Fabre, and A. Maître, Phys. Rev. Lett. **100**, 013604 (2008).
[14] W. Imajuku, A. Takada, and Y. Yamabayashi, Electron. Lett. **35**, 1954 (1999).
[15] M. Marhic, C. Hsia, and J.-M. Jeong, Electron. Lett. **27**, 210 (1991).
[16] Z. Tong *et al.*, Nat. Photonics **5**, 430 (2011).
[17] K. Croussore and G. Li, IEEE Photon. Technol. Lett. **19**, 864 (2007).
[18] R. Tang, P. S. Devgan, V. S. Grigoryan, P. Kumar, and M. Vasilyev, Opt. Express **16**, 9046 (2008).
[19] M. I. Kolobov and L. A. Lugiato, Phys. Rev. A **52**, 4930 (1995).
[20] E. Lantz and F. Devaux, IEEE J. Sel. Topics Quantum Electron. **14**, 635 (2008).
[21] M. Vasilyev, N. Stelmakh, and P. Kumar, Opt. Express **17**, 11415 (2009).
[22] V. Boyer, A. M. Marino, R. C. Pooser, and P. D. Lett, Science **321**, 544 (2008).
[23] N. Corzo, A. M. Marino, K. M. Jones, and P. D. Lett, Opt. Express **19**, 21358 (2011).
[24] U. L. Andersen and G. Leuchs, J. Mod. Opt. **54**, 2351 (2007).
[25] R. C. Pooser, A. M. Marino, V. Boyer, K. M. Jones, and P. D. Lett, Phys. Rev. Lett. **103**, 010501 (2009).
[26] C. F. McCormick, A. M. Marino, V. Boyer, and P. D. Lett, Phys. Rev. A **78**, 043816 (2008).
[27] P. M. Vaughan and R. Trebino, Opt. Express **19**, 8920 (2011).